JOURNAL OF AIRCRAFT
Vol. 31, No. 3, May–June 1994

Leading-Edge Vortex Breakdown for Wing Planforms with the Same Slenderness Ratio

William A. Straka*
George Washington University, Hampton, Virginia 23681
and
Michael J. Hemsch†
Lockheed Engineering & Sciences Company, Hampton, Virginia 23666

A dye flow visualization investigation was conducted on two sets of wing planforms to better understand the effects of planform shaping on leading-edge vortex breakdown. The first set of planforms consisted of five cropped planforms, including a 66.3-deg delta, 80/55 double-delta, and three blended 80/55 double-deltas. The second set of planforms consisted of nine planforms of the same slenderness ratio, including a 69.3-deg delta, two gothics, three double-deltas, and three corresponding blended double-deltas. Results of these experiments have indicated that planforms with a common slenderness ratio develop quite similar characteristics for breakdown of the apex vortex at the trailing edge. It was found that planform shaping significantly alters the forward progression of breakdown along the wing as angle of attack is increased. The effect of increasing filleting to double-delta planforms was shown to degrade the apex vortex breakdown characteristics of the planforms. Also, it was found that by moving the kink location of the double-delta aft on the planform, breakdown characteristics are improved.

Nomenclature

b = wing span
c_r = root chord of exposed wing panel, 9.483 in.
c_x = root chord of planform forward of cropped tip, 8.556 in.
P = planform area parameter, Eq. (3)
Re_{cr} = Reynolds number, based on root chord
s = local exposed semispan
s_{TE} = exposed semispan at trailing edge
$s_{0.25cr}$ = exposed semispan at location of $0.25c_r$
SR = slenderness ratio, Eq. (1)
(x, y, z) = body axis coordinate system, origin at wing-body apex juncture
$\bar{x}$ = nondimensional chordwise planform coordinate, x/c_r
$\hat{x}$ = nondimensional chordwise planform coordinate, x/c_x
x_k = chordwise location of double-delta leading-edge kink measured from wing apex
$\bar{y}$ = nondimensional spanwise planform coordinate, y/c_r
$\hat{y}$ = nondimensional spanwise planform coordinate, y/c_x
α = angle of attack
α_0 = angle of attack at which wing and strake vortex begin to interact and merge
β = sideslip angle
κ = ratio of double-delta discontinuity location to root chord, x_k/c_r
Λ_{core} = vortex core sweep angle, deg
Λ_{LE} = delta wing leading-edge sweep angle, deg
$\Lambda_{LE(0.25cr)}$ = equivalent delta wing leading-edge sweep angle, $\tan^{-1}(s_{0.25cr}/c_r)$
Λ_s = strake leading-edge sweep angle, deg
Λ_w = wing leading-edge sweep angle, deg

Received Feb. 9, 1993; revision received March 28, 1993; accepted for publication July 21, 1993. This paper is declared a work of the U.S. Government and is not subject to copyright protection in the United States.

*Graduate Assistant, JIAFS Program, M/S 269; currently Research Assistant, Applied Research Laboratory, The Pennsylvania State University, P.O. Box 30, State College, PA 16804. Member AIAA.
†Engineer, Staff, 144 Research Drive. Associate Fellow AIAA.

Introduction

THE importance of leading-edge vortex flows to slender aircraft has been well-documented in recent years.[1–3] As a result, the aerodynamic characteristics of leading-edge vortex flows have been extensively studied both experimentally and computationally. Much of this research has been in the area of vortex breakdown, the sudden and dramatic change in the flow which results in the turbulent dissipation of the vortex. Various authors[4–10] have conducted parametric studies on the many factors influencing the vortex breakdown on delta wings. Some of those factors include aspect ratio,[4,5] camber,[4,6] cropping,[6,7] flaps,[8,9] surface roughness,[10] and trailing-edge geometry.[6,7] Very little systematic work, however, has been done on configurations other than delta or double-delta planforms. The purpose of this investigation is to experimentally compare vortex properties of various unconventional planform wings. This is, to the authors' knowledge, the first systematic investigation comparing breakdown characteristics of several families of planforms while maintaining a common slenderness ratio. The motivation of this research was to gain a better understanding of the effects that planform leading-edge shaping has on leading-edge vortex breakdown.

Experimental Details

Facility Description

The experiment was conducted in the NASA Langley Research Center (LaRC) water tunnel.[11] The wing planform configurations used in this study were installed in the vertically arranged 16- × 24-in. test section so that the wing plane was parallel to the 16-in. side at an angle of attack of 0 deg. The test section was equipped with a C-strut pitch mechanism which allows for angle-of-attack ranges of −30 to +30 deg. For the present investigation, a 30-deg offset model support sting was used to allow for higher angles of attack ranging from $\alpha \simeq 0$ to 45 deg. Figure 1 illustrates this support setup. The upper limit of angle of attack was set by model proximity

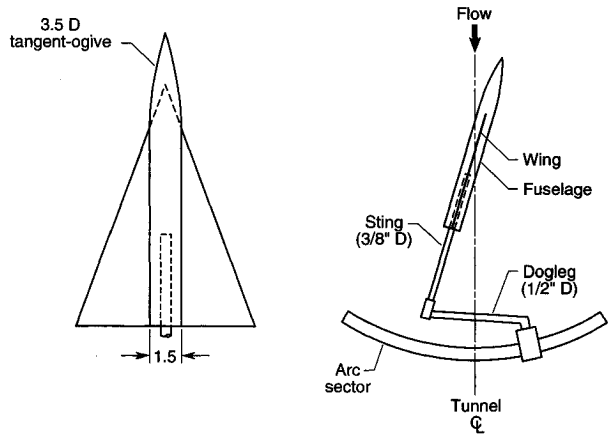

Fig. 1 Model mounting and support system.

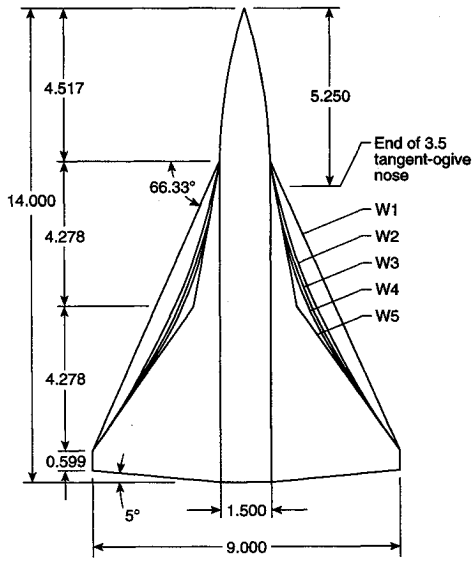

Fig. 2 Model dimensions (in.) of planform configurations *W1–W5*.

to the wall. For the present series of tests, the test section velocity was held at 0.25 ft/s to minimize the freestream flow turbulence and allow for undissipated dye flow visualization. The resulting Re_{cr} was approximately 1.85×10^4 for each of the models tested. Although this Reynolds number is small relative to flight values, Erickson[5] observed that the variation in vortex breakdown at different Reynolds numbers to be no greater than the differences observed at the same Reynolds number during different experiments.

Model Description

The present investigation involved testing a total of 14 different wing planform configurations. To adequately compare the effects of leading-edge planform shaping, certain geometric constraints were introduced. The primary constraint used in developing planform configurations was to hold constant the exposed wingtip semispan s_{TE} and the root chord c_r. By keeping a constant slenderness ratio

$$SR = (s_{TE}/c_r) \tag{1}$$

planform configuration changes were reduced to leading-edge shaping changes only. In addition, a minimum wing sweep angle $\Lambda_w = 55$ deg, and a maximum strake sweep angle $\Lambda_s = 80$ deg, were chosen to provide a planform consistent with modern high-speed/high-agility fighter aircraft. Each planform was made out of a 0.050-in.-thick, flat aluminum sheet to obtain a near "zero thickness" and to eliminate both camber and thickness effects. Each of the wing-planform configurations were mounted on a 14-in.-long axisymmetric body with a 3.5 tangent-ogive forebody and a 1.5-in.-diam cylindrical aft body. This was done to reduce the possibility of wing vortex asymmetries and to more fully represent "real world" aircraft configurations. Each of these wing-body configurations were supported by a $\frac{3}{8}$-in.-diam model dogleg sting at the centerline of the axisymmetric body and then mounted in the tunnel to the C-strut angle-of-attack mechanism.

The first set of planforms included were the five planform configurations, *W1–W5*, illustrated in Fig. 2. Each of these planforms included cropped tips as well as 5 deg of trailing-edge forward sweep. Each planform was designed with the same 9.843-in. root chord and 9.0-in. span which led to a common slenderness ratio $SR = 0.395$. An 80/55/0.45 (i.e., $\Lambda_s = 80$ deg, $\Lambda_w = 55$ deg, and $\kappa = 0.45$) cropped double-delta *W5* was chosen as the baseline configuration. Three blended planforms, *W2–W4*, with concave leading-edge shaping were derived by changing the degree of apex to tip filleting on the baseline planform. A cropped delta planform *W1* with a leading-edge sweep $\Lambda_w = 66.3$ deg, was also included in this first series of tests. Details of the various planforms are summarized in Table 1. The nondimensional equations of the leading-edge sections are given in the Appendix.

After the first set of planforms were tested, it was decided to further investigate the effects of planform shaping while constraining the planform slenderness ratio. A total of nine configurations (*W6–W14*) were included in this second set of planforms. To reduce the number of configuration parameters, these nine models were designed without both the cropped

Table 1 Geometric details of the various planform configurations

Configuration	Planform type	*SR*	*P*	*k*
W1	Delta	0.395	0.500[a]	0.000[a]
W2	Concave	"	0.403[a]	—
W3	Concave	"	0.382[a]	—
W4	Concave	"	0.371[a]	—
W5	Double-delta	"	0.350[a]	0.500[a]
W6	Delta	0.377	0.500	0.000
W7	Double-delta	"	0.418	0.307
W8	Double-delta	"	0.367	0.500
W9	Double-delta	"	0.336	0.616
W10	Gothic	"	0.666	—
W11	Gothic	"	0.582	—
W12	Concave	"	0.430	—
W13	Concave	"	0.412	—
W14	Concave	"	0.370	—

[a]Based on chord c_r.

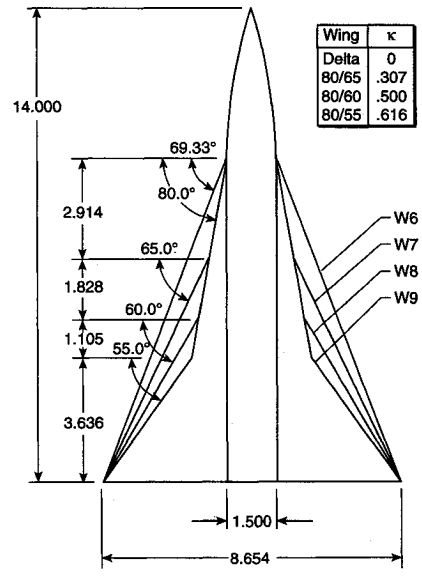

Fig. 3 Model dimensions (in.) of double-delta planform configurations *W6–W9*.

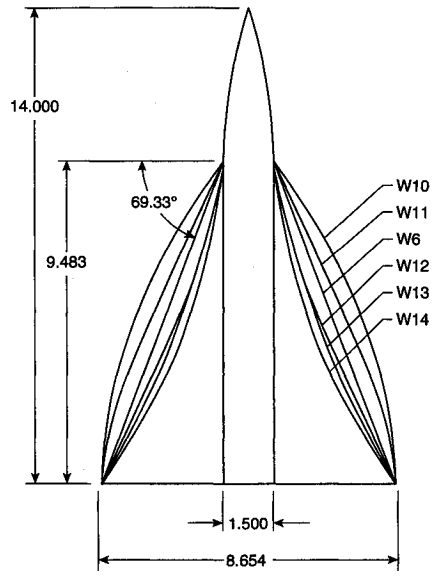

Fig. 4 Model dimensions (in.) of unconventional planform configurations *W10–W14*.

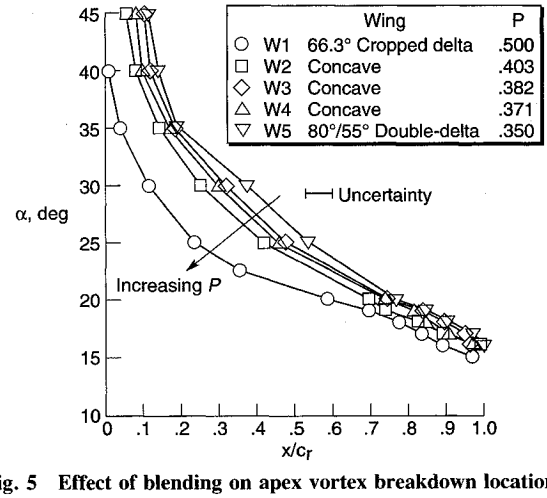

Fig. 5 Effect of blending on apex vortex breakdown locations.

section and the trailing-edge sweep used in the first five models. Planforms *W6–W9* are illustrated in Fig. 3. These were designed to determine the effect of moving the leading-edge kink location κ on double-delta configurations with the same slenderness ratio of $SR = 0.377$. The double-delta configurations were designed by keeping the forward panel (strake) sweep constant at $\Lambda_s = 80$ deg, and changing the aft panel (wing) sweep to $\Lambda_w = 55$, 60, and 65 deg. This resulted in three double-delta planforms with the same slenderness ratio and different leading-edge kink locations κ. A delta planform *W6* with a leading-edge sweep $\Lambda_w = 69.3$ deg, was also included. Five unconventional wing planforms ranging from those with concave leading-edge shapes to gothic (convex leading-edge shaped) style planforms, were also tested. These are illustrated in Fig. 4. The three concave planforms, *W12–W14*, each represent a filleting of the previous double-delta planforms, *W7–W9*. Equations for the curved sections were developed by parabolically blending the wing and strake on each double-delta. The nondimensional planform equations of the leading-edge shaping are given in the Appendix. The planform parameters are summarized in Table 1.

Test Procedure

A pressurized dye injection system was used for flow visualization. To entrain dye into the core in order to visualize the leading-edge vortex trajectory and its breakdown, dye ports were placed on the windward side of the model planforms at the apex of each planform leading edge. On the double-delta planforms *W7–W9*, a second dye port was placed at the leading-edge kink or juncture between the strake and wing. This enabled visualization of the wing vortex as well as the vortex originating from the apex (i.e., strake vortex). Location measurements of vortex breakdown were facilitated by a grid laid out on the wing planforms. Videotape and still film photography were used during the test program to document the leading-edge vortex trajectory and breakdown locations. Early in the investigation, it was determined from dye issuing from ports near the apex of the forebody that the influence of the weak fuselage-shed vorticity on the wing vortex breakdown characteristics was minimal. Previous work by Hall[12,13] confirms this result.

Experimental Results (Cropped Planforms)

The first portion of this investigation included testing the five cropped planforms, *W1–W5*, shown in Fig. 2. Breakdown locations of the apex leading-edge vortex were measured using dye visualization at 5-deg intervals for angles of attack ranging from $\alpha = 15$ to 45 deg, and then from $\alpha = 45$ to 15 deg to account for any hysteresis effects. Smaller angle-of-attack intervals were used at various stages in the test program to determine more precisely at what angle of attack breakdown at the trailing edge occurred. Each planform was tested at a sideslip condition of $\beta = 0$ deg.

Breakdown Results

Mean values of breakdown locations for each of these planforms are shown in Fig. 5 as a fraction of the root chord. A value of $x/c_r = 1.0$ corresponds to a location at the wing-planform trailing edge and a value, $x/c_r = 0.0$ to a location at the apex of the wing. It should be noted that breakdown characteristics of a planform are improved when this curve is shifted upwards resulting in a higher achievable angle-of-attack envelope. It is, therefore, of great importance that the presence of the fuselage causes vortex breakdown to occur (for the same x/c_r) at up to 10 deg lower angle of attack.[14]

A key feature determined by this experiment is that the breakdown of the leading-edge vortex at the trailing edge of these wing configurations occurred at nearly identical angles of attack. For the double-delta, delta, and each concave planform, trailing-edge breakdown occurred in the angle-of-attack range 15–16 deg. As can be seen, the main effect of filleting on the vortex breakdown appears to be on the forward progression of breakdown along the wing with increasing angles of attack. As the amount of fillet area added to the baseline planform *W5* is increased, the breakdown characteristics of the apex-originated vortex were degraded. For instance, at an angle of attack of 25 deg, the double-delta had a mean vortex burst location at about 55% of the root chord. For the concave blended planforms at the same angle of attack, vortex burst occurred between 5–10% closer to the wing apex, and on the delta at approximately the 25% root chord point. The planform blending of the strake and the wing appeared to eliminate the outboard wing leading-edge vortex typically present on double-delta planforms with only a single leading-edge vortex (characteristic of a plain delta wing) being observed. This resulting single (apex) leading-edge vortex of the blended planforms led to improved breakdown over that of the plain delta planform *W1*, without the typical double-delta outboard wing vortex breakdown and interactions.

An alternative method for correlating the vortex breakdown data of configurations *W1–W5* is presented in Fig. 6. The breakdown angles of attack for the various configurations are given as a function of the nondimensional local semispan s/s_{TE}, corresponding to the axial location of breakdown x/c_r, given in Fig. 5. As can be seen, this approach collapses the breakdown data of the various configurations much better, particularly for the forward half of the wing. Variations in the data in the region of $s/s_{TE} = 1.0$ are probably the result of the planform cropping.

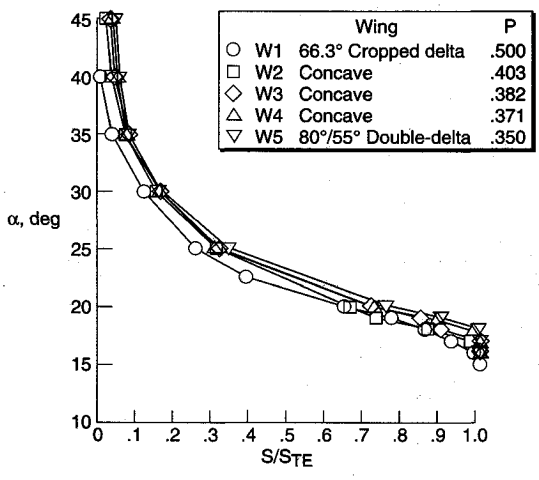

Fig. 6 Vortex breakdown angle of attack as a function of exposed semispan for configurations *W1–W5*.

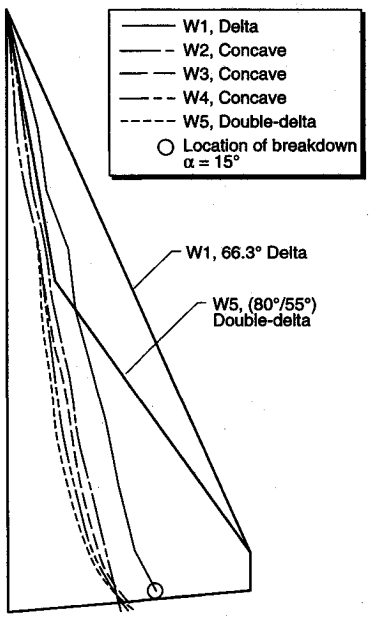

Fig. 7 Effect of blending on vortex core trajectory (α = 15 deg).

Vortex Trajectory

Vortex core trajectories for each test condition and configuration were estimated by frame-by-frame analysis of the videotape recordings. In using this method of data retrieval, projection errors due to angle-of-attack changes are not accounted for. Estimated mean values of the vortex locations were used to account for core unsteadiness. Representative trajectories at a single angle of attack of 15 deg are sketched in Fig. 7 for each of the five planform cores as determined from the videotape analysis. The outline of the delta *W1*, and double-delta *W5*, planforms are given to provide a basis of comparison. Analysis of these results and other trajectories not shown, revealed that for a given planform configuration vortex core trajectory is relatively insensitive to angle-of-attack changes. On double-delta planforms this insensitivity occurred only for angles of attack above which the strake and wing leading-edge vortices combine (a phenomenon discussed later). This angle-of-attack insensitivity is in agreement with Erickson's results for delta planforms.[4] The results presented in Fig. 7 also demonstrate that adding fillet area to the baseline double-delta tends to decrease the core trajectory sweep angle Λ_{core}.

The above observations that the core trajectory sweep decreases with increasing fillet area are very similar to results obtained by Erickson[4] for delta wing core trajectories when the leading-edge sweep is reduced. Consequently, the vortex

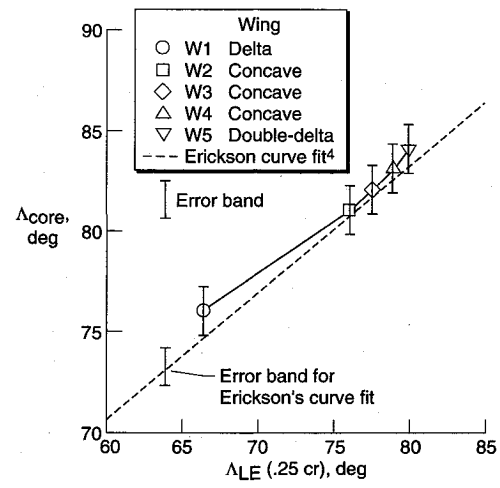

Fig. 8 Effect of planform leading-edge sweep on vortex core trajectory.

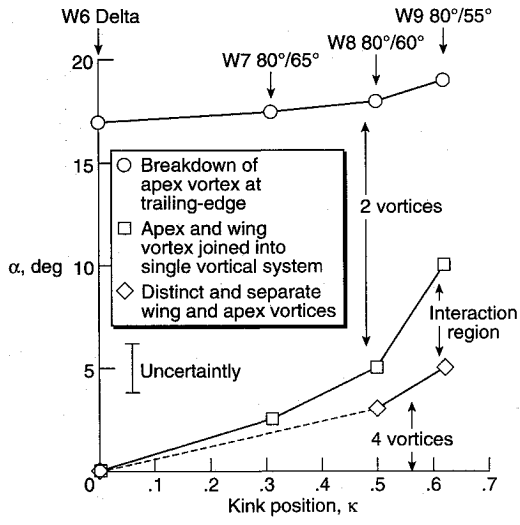

Fig. 9 Effect of kink position on double-delta vortex formation.

core trajectories of the blended planforms have been compared with a modified version of Erickson's curve-fit for plain delta wings given by

$$\Lambda_{core} = 33.5 + 0.62\Lambda_{LE} \tag{2}$$

In order to compare the blended planforms with Erickson's empirical curve fit, $\Lambda_{LE(0.25cr)}$, based on the first 25% of the exposed root chord was obtained for each planform. Values of the leading-edge vortex core sweep were measured at various angles of attack. A straight line approximation of the core trajectory was used to determine the core sweep angle for each planform. As mentioned previously, the vortex core trajectory exhibited very little angle-of-attack sensitivity. Therefore, data at a lower angle of attack was used to reduce projection errors. The vortex core trajectories given as a function of equivalent sweep are compared to Erickson's delta-wing core trajectory equation in Fig. 8. The resulting data of the present investigation falls within a 95% confidence error bound of the curve fit as estimated from the data given in Erickson.[4] This result suggests that the apex region dominates the determination of leading-edge vortex properties and breakdown characteristics.

Experimental Results (Uncropped Planforms)

The second part of this investigation included testing the nine uncropped planforms *W6–W14* as shown in Figs. 3 and 4. Breakdown locations of the apex-originated leading-edge

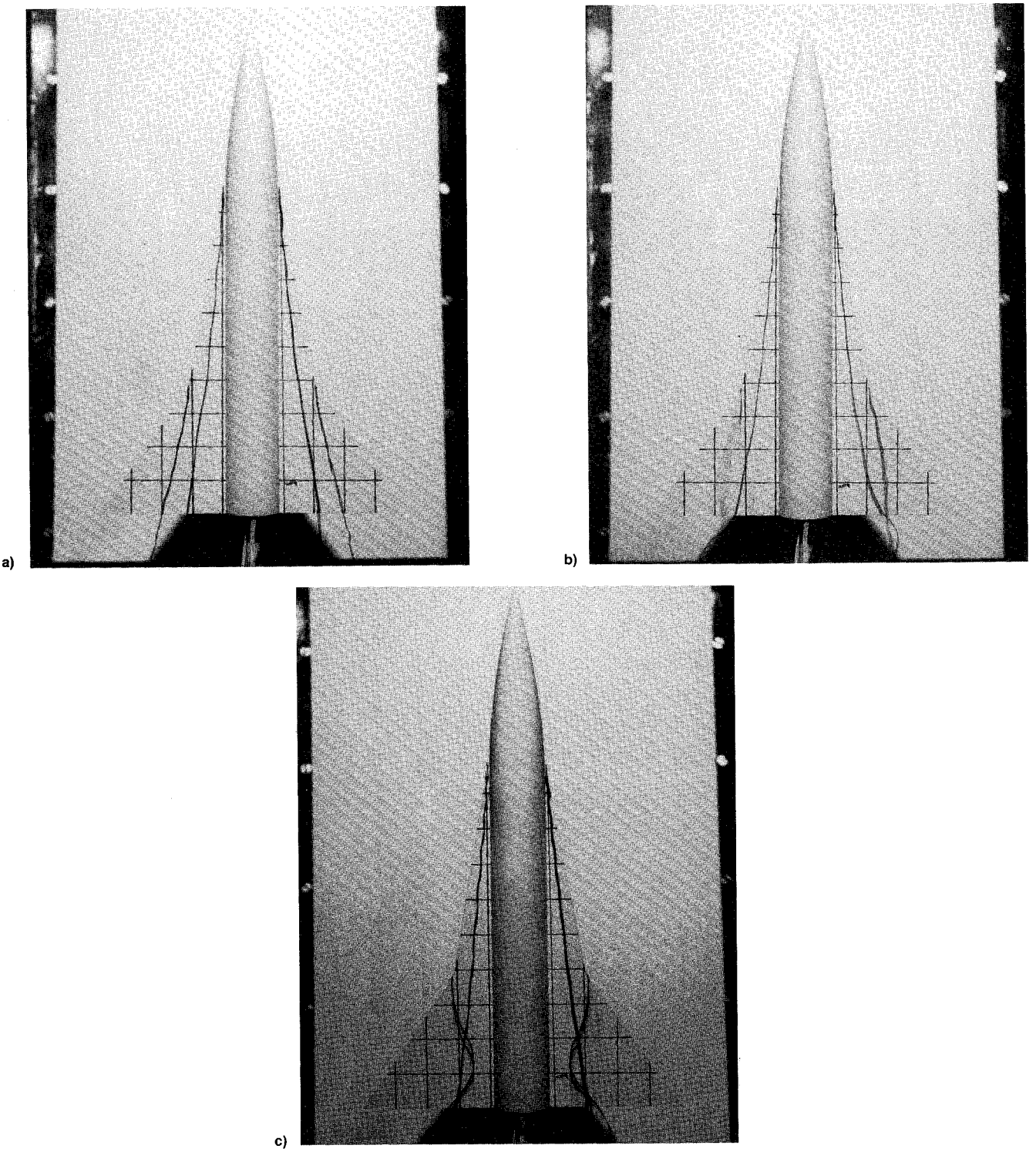

Fig. 10 Vortex core trajectories over 80/55-deg double-delta planform *W*9: α = a) 5.0, b) 7.5, and c) 10.0 deg.

vortex were measured at 2.5-deg intervals for angles of attack ranging from α = 10 to 42.5 deg, and from α = 42.5 to 10 deg. The wing leading-edge vortex originating from the leading-edge kink of the double-delta planforms were also visualized to determine the conditions at which strong interactions occur between the strake and the wing vortex. Such interactions typically began at angles of attack less than 10 deg. Once the interaction starts at some α_0, it continues for all $\alpha \geq \alpha_0$. Each planform was tested at a sideslip condition of β = 0 deg.

Double-Delta Vortex Formation

A series of tests were completed to investigate the effect of moving the leading-edge kink location κ, while retaining an identical slenderness ratio on a plain delta *W*6, and three double-delta planforms *W*7–*W*9. Figure 9 illustrates how the flow pattern on these planforms is affected by changes in both angle of attack and leading-edge kink position. At a very small angle of attack, the strake vortex is initially fed by vorticity shed by the strake leading edge. Downstream of the leading-edge kink, feeding into the strake vortex no longer occurs, as all the shed vorticity flows into the wing vortex. This flow pattern is represented in Fig. 9 by the lower region labeled "4 vortices." Figure 10a illustrates this vortex flowfield pattern when both the wing and apex vortices are separate and distinct.

As angle of attack was increased, the two vortices began to interact over the wing. Initially, the strake vortex is sucked

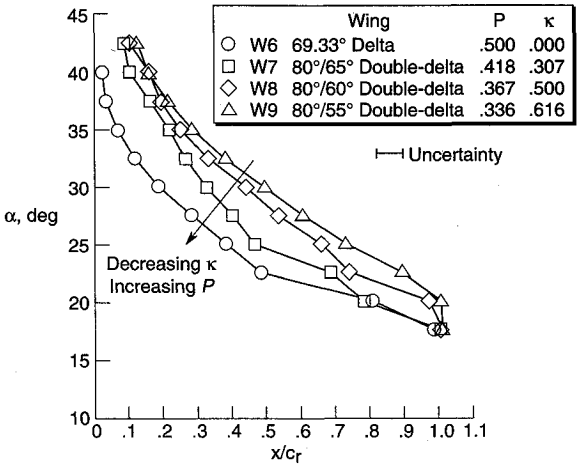

Fig. 11 Effect of kink placement on vortex breakdown locations of double-delta planforms.

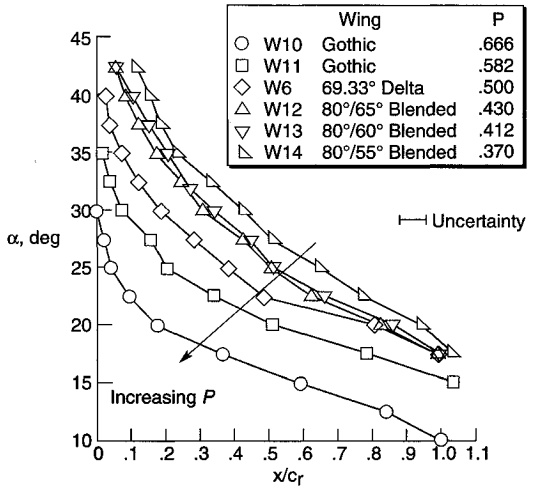

Fig. 12 Effect of area changes on vortex breakdown locations of planforms with same slenderness ratio.

outward towards the wing vortex. This is due to the stronger relative strength of the wing vortex which dominates the interaction. The interaction is represented by the narrow band between the diamond and square symbols in Fig. 9 and is illustrated in the photograph in Fig. 10b. In this transition region, both the wing and the strake vortices still have their own distinct cores.

As angle of attack is further increased, the strake vortex begins to dominate the flowfield. The vorticity shed on the outboard wing panel is fed into the strake vortex core before it is able to wind up around itself. At this angle of attack, represented by the square symbols in Fig. 9, the last remains of the original four-vortex system disappears and a two-vortex system is present. This leads to a single vortical region similar to the flowfield above a plain delta wing. Figure 10c illustrates the joined vortical flowfield. The strake vortex has returned to the trajectory it had at $\alpha = 5$ deg, and the dye filament from the leading-edge discontinuity flows around the strake core in a spiral manner.

The vortex formation summarized in Fig. 9 can be seen to be also dependent on leading-edge kink location. With increasing distance of the leading-edge discontinuity from the wing apex, the onset of the above vortex formation and interactions are delayed towards higher angles of attack. This is due to the fact that, for planforms with constant slenderness ratio, increasing the distance from the wing apex to the kink location κ results in smaller wing sweep angles Λ_w, and therefore a stronger, more outboard, wing vortex. Observations by Brennenstuhl and Hummel[15] appear to confirm this trend. However, the actual values obtained in the present investigation do not agree with those of Brennenstuhl and Hummel who measured these trends at approximately 10 deg higher angle of attack. Although it was not quantified, the discrepancy was probably due to a combination of the 3.5 tangent-ogive-cylinder body, support interference effects, and the difference in Reynolds number between the investigations. Straka and Hemsch[14] showed that fuselage-induced upwash can dramatically influence the breakdown angle of attack, and Thompson[16] documented a high degree of Reynolds number dependence in double-delta strake/wing vortex interactions and merging.

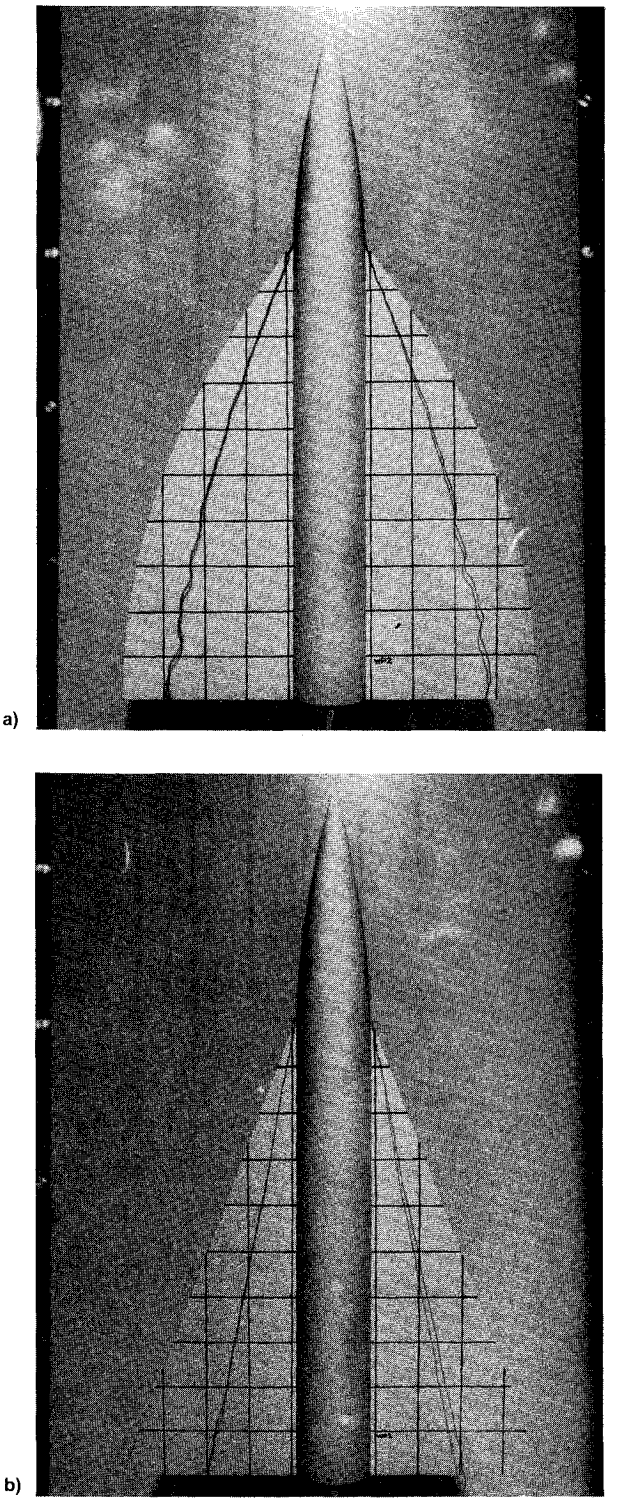

Fig. 13 Effect of planform on vortex core trajectory characteristics: a) gothic planform *W10* at $\alpha = 7.5$ deg and b) delta planform *W6* at $\alpha = 15.0$ deg.

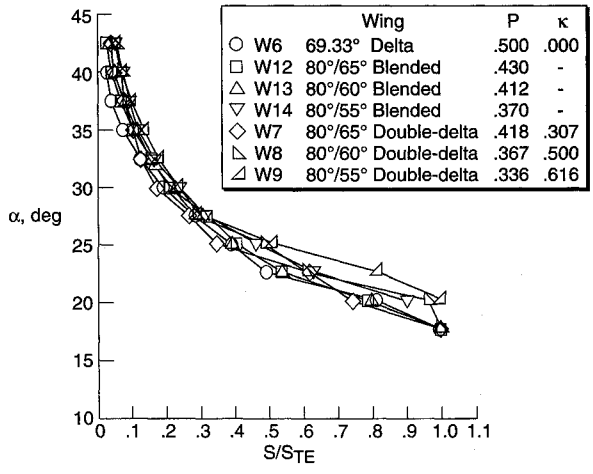

Fig. 14 Vortex breakdown angle of attack as function of exposed semispan.

Double-Delta Vortex Breakdown

Mean values of breakdown locations for the apex-originated leading-edge vortex for the delta planform *W6*, and each of the double-deltas *W7*–*W9*, are shown in Fig. 11. The key feature is the result that breakdown at the trailing edge of each of the configurations occurred at approximately the same angle of attack. This can be more easily seen in Fig. 9, where breakdown of the apex vortex at the planform trailing edge is represented by the curve denoted with circle symbols. This effect was also documented in the results of Brennenstuhl and Hummel.[15]

As can be seen in Fig. 11, the main effect that moving the kink position aft has on apex (strake) vortex breakdown appears to be in delaying breakdown over the wing at a particular chordwise location. As the distance of the leading-edge kink from the apex is increased, the breakdown curves tend to shift upward. This results in dramatically improved breakdown characteristics for the configurations with higher values of κ.

Unconventional Planform Vortex Breakdown

The six planforms shown in Fig. 4 were tested to investigate the effect of planform area changes on the vortex breakdown characteristics of planforms with the same slenderness ratio. In the analysis of these wing planform configurations, it was found that Squire's planform area parameter[17]

$$P = \frac{\text{exposed planform area}}{2s_{TE}c_r} \tag{3}$$

was useful for comparison purposes. This parameter is the ratio of exposed wing area to the area of an enclosing rectangle of the same exposed span and root chord.

Mean values of vortex burst locations for each of these planforms at zero sideslip are shown in Fig. 12. For configurations with P of less than or equal to an equivalent plain delta or 0.5, trailing-edge breakdown occurred at a common angle of attack. However, this trend does not hold for planforms with $P > 0.5$ (gothic). Also of interest regarding the gothic planforms is that the vortex core appeared much more unsteady than those with $P \leq 0.5$. This unsteadiness is evident even before breakdown approaches the trailing edge as illustrated in Fig. 13a. The vortex core appears unsteady and meanders at locations greater than 50% chord, as shown by the waviness of the dye trajectory in the photograph. This is not the case on the delta planform as shown in Fig. 13b. It is conjectured that the associated unsteadiness in the gothic planform cores is probably the result of the slowly increasing pressure imposed on the core by the reduction in local sweep as the trailing edge is approached.[18]

As the planform area is increased holding the slenderness ratio constant, the vortex breakdown characteristics are adversely affected. This is demonstrated in Fig. 12 in the forward progression of vortex burst along the wing with increasing angle of attack. The planforms with the lower values of P exhibit better breakdown characteristics.

There are two ways to change a planform's aspect ratio, and therefore, the aerodynamic properties such as lift and drag. The first is by changing the planform chord or span (i.e., sweep), and the second by changing the planform area (i.e., leading-edge shaping). The first method has been studied previously and results in drastic changes in the leading-edge vortex breakdown characteristics of the wing.[5] The second method, studied in the present investigation, shows that a wing planform leading-edge shape may be changed without drastically effecting the high angle-of-attack vortex breakdown characteristics at the trailing edge.

The breakdown data can be replotted as a function of the nondimensional local semispan s/s_{TE}, corresponding to the axial location of breakdown. This correlation is shown in Fig. 14 for configurations *W6*–*W9* and *W12*–*W14*. Again, this method of presenting the breakdown data correlates the data fairly well for delta, double-delta, and concave planforms. However, the breakdown data of the gothic planforms *W10* and *W11* did not collapse like those with $P \leq 0.5$.

Conclusions

The vortex breakdown characteristics of various unconventional wing planforms with the same slenderness ratios were systematically studied using dye flow visualization techniques in the NASA Langley Research Center water tunnel. This investigation provided a means to better understand the effects of planform shaping on the formation and breakdown of the leading-edge vortex originating at the apex.

First, it was found that on planforms with the same slenderness ratio, breakdown at the trailing edge occurs at approximately the same angle of attack for planforms with area less that an equivalent delta or $P \leq 0.5$. The forward progress of breakdown on the wing with increasing angle of attack was shown to be improved by decreasing the area of the wing. Of the configurations without leading-edge discontinuities, those with the largest areas (i.e., gothics) exhibited vortex breakdown at lower angles of attack, while concave or blended planform were found to increase the angle of attack at which vortex breakdown occurs.

Second, on double-delta planforms, filleting the strake and wing to eliminate the leading-edge discontinuity was found to adversely affect the forward progression of vortex breakdown. The addition of fillet area to a baseline double-delta was also found to decrease the core trajectory sweep angle. Increasing the distance of the leading-edge discontinuity from the wing apex on double-deltas of the same slenderness ratio delayed breakdown over the wing at a particular chordwise location, and shifted strake and wing interactions, such as vortex merging, to a higher angle of attack.

Appendix

The nondimensional planform equations are given below for each configuration:

W1:

$$\hat{y} = \hat{x}(\tan 23.67 \text{ deg}) \tag{A1}$$

W2:

$$\hat{y} = 0.5\hat{x}^2(\tan 35 \text{ deg} - \tan 10 \text{ deg}) + \hat{x}(\tan 10 \text{ deg}) \tag{A2}$$

W3:

$$\hat{y} = (-0.5\hat{x}^4 + \hat{x}^3)(\tan 35 \text{ deg} - \tan 10 \text{ deg}) + \hat{x}(\tan 10 \text{ deg}) \tag{A3}$$

*W*4:

$$\hat{y} = (-2.5\hat{x}^8 + 10\hat{x}^7 - 14\hat{x}^6 + 7\hat{x}^5)(\tan 35 \text{ deg} - \tan 10 \text{ deg}) + \hat{x}(\tan 10 \text{ deg}) \quad \text{(A4)}$$

*W*5:

$$\hat{y} = \hat{x}(\tan 10 \text{ deg}), \quad \hat{x} \le 0.5 \quad \text{(A5)}$$

$$\hat{y} = \hat{x}(\tan 35 \text{ deg}) - 0.5(\tan 35 \text{ deg} - \tan 10 \text{ deg}), \quad \hat{x} \ge 0.5 \quad \text{(A6)}$$

*W*6:

$$\bar{y} = \bar{x}(\tan 20.67 \text{ deg}) \quad \text{(A7)}$$

*W*7:

$$\bar{y} = \bar{x}(\tan 10 \text{ deg}), \quad \bar{x} \le 0.307 \quad \text{(A8)}$$

$$\bar{y} = \bar{x}(\tan 25 \text{ deg}) - 0.307(\tan 25 \text{ deg} - \tan 10 \text{ deg}), \quad \bar{x} \ge 0.307 \quad \text{(A9)}$$

*W*8:

$$\bar{y} = \bar{x}(\tan 10 \text{ deg}), \quad \bar{x} \le 0.500 \quad \text{(A10)}$$

$$\bar{y} = \bar{x}(\tan 30 \text{ deg}) - 0.500(\tan 30 \text{ deg} - \tan 10 \text{ deg}), \quad \bar{x} \ge 0.500 \quad \text{(A11)}$$

*W*9:

$$\bar{y} = \bar{x}(\tan 10 \text{ deg}), \quad \bar{x} \le 0.616 \quad \text{(A12)}$$

$$\bar{y} = \bar{x}(\tan 35 \text{ deg}) - 0.616(\tan 35 \text{ deg} - \tan 10 \text{ deg}), \quad \bar{x} \ge 0.616 \quad \text{(A13)}$$

*W*10:

$$\bar{y} = (2.0\bar{x} - \bar{x}^2)(\tan 20.67 \text{ deg}) \quad \text{(A14)}$$

*W*11:

$$\bar{y} = (1.25\bar{x} - 0.25\bar{x}^5)(\tan 20.67 \text{ deg}) \quad \text{(A15)}$$

*W*12:

$$\bar{y} = 0.814\bar{x}^2(\tan 25 \text{ deg} - \tan 10 \text{ deg}) + \bar{x}(\tan 10 \text{ deg}), \quad \bar{x} \le 0.615 \quad \text{(A16)}$$

$$\bar{y} = \bar{x}(\tan 25 \text{ deg}) - 0.307(\tan 25 \text{ deg} - \tan 10 \text{ deg}), \quad \bar{x} \ge 0.615 \quad \text{(A17)}$$

*W*13:

$$\bar{y} = 0.5\bar{x}^2(\tan 30 \text{ deg} - \tan 10 \text{ deg}) + \bar{x}(\tan 10 \text{ deg}) \quad \text{(A18)}$$

*W*14:

$$\bar{y} = \bar{x}(\tan 10 \text{ deg}), \quad \bar{x} \le 0.233 \quad \text{(A19)}$$

$$\bar{y} = 0.041 + (0.652\bar{x}^2 - 0.304\bar{x} + 0.035)(\tan 35 \text{ deg} - \tan 10 \text{ deg}) + (\bar{x} - 0.233)(\tan 10 \text{ deg}), \quad \bar{x} \ge 0.233 \quad \text{(A20)}$$

Acknowledgments

The authors gratefully acknowledge the support of the Transonic Aerodynamics Branch at NASA Langley Research Center, the first author through George Washington University's JIAFS program and the second through Contract NAS1-19000.

References

[1]Polhamus, E. C., "Applying Slender Wing Benefits to Military Aircraft," *Journal of Aircraft*, Vol. 21, No. 8, 1984, pp. 545–558.

[2]Polhamus, E. C., "Vortex Lift Research: Early Contributions and Some Current Challenges," *Vortex Flow Aerodynamics*, Vol. 1, NASA CP 2416, Paper 1, 1986, pp. 1–30.

[3]Lamar, J. E., "Non Linear Lift Control at High Speed and High Angle of Attack Using Flow Technology," *Special Course on Fundamentals of Fighter Aircraft Design*, AGARD Rept. 740, Rhode-St-Genese, Belgium, Feb. 1986.

[4]Erickson, G. E., "Flow Studies of Slender Wing Vortices," AIAA Paper 80-1423, July 1980.

[5]Erickson, G. E., "Vortex Flow Correlation," AFWAL-TR-80-3143, Wright-Patterson AFB, OH, Jan. 1981.

[6]Thompson, D. H., "A Water Tunnel Study of Vortex Breakdown over Wings with Highly Swept Leading Edges," Aeronautics Research Labs., Aerodynamics Note 356, Melbourne, Australia, May 1975.

[7]Wentz, W. H., "Wind Tunnel Investigations of Vortex Breakdown on Slender Sharp-Edged Wings," Ph.D. Dissertation, Univ. of Kansas, Lawrence, KS, 1969.

[8]Lambourne, N. C., and Bryer, D. W., "The Bursting of Leading Edge Vortices—Some Observations and Discussion of the Phenomenon," Aeronautical Research Council Repts. and Memoranda 3282, April 1961.

[9]Erickson, G. E., "Water Tunnel Studies of Leading-Edge Vortices," *Journal of Aircraft*, Vol. 19, No. 6, 1982, pp. 442–448.

[10]Wentz, W. H., and Kohlman, D. L., "Vortex Breakdown on Slender Sharp-Edged Wings," AIAA Paper 69-778, July 1969.

[11]Pendergraft, O. C., Jr., Neuhart, D. H., Kariya, T. T., "A User's Guide to the Langley 16- by 24-Inch Water Tunnel," NASA TM 104200, Jan. 1992.

[12]Hall, R. M., "Influence of Forebody Cross-Sectional Shape on Wing Vortex-Burst Location," *Journal of Aircraft*, Vol. 24, No. 9, 1987, pp. 645–652.

[13]Hall, R. M., and Del Frate, J. H., "Interaction Between Forebody and Wing Vortices—A Water Tunnel Study," Air Force Wright Aeronautical Lab. TM-85-252, Wright-Patterson Air Force Base, OH, Jan. 1986.

[14]Straka, W. A., and Hemsch, M. J., "Effect of a Fuselage on Delta Wing Vortex Breakdown," *Journal of Aircraft* (to be published).

[15]Brennenstuhl, U., and Hummel, D., "Vortex Formation over Double-Delta Wings," *Proceedings of the 13th Congress of International Council of the Aerospace Sciences*, Vol. 2, ICAS-82-6.6.3, Aug. 1982, pp. 1133–1146.

[16]Thompson, D. H., "Visualisation of Vortex Flows Around Wings with Highly-Swept Leading-Edges," 9th Australasian Fluid Mechanics Conf., Auckland, New Zealand, Dec. 1986.

[17]Squire, L. C., "Experimental Work on the Aerodynamics of Integrated Slender Wings for Supersonic Flight," *Progress in Aerospace Sciences*, Vol. 20, No. 1, 1981, pp. 1–96.

[18]Straka, W. A., "Effects of Wing Planform Shaping on Leading-Edge Vortex Breakdown Characteristics," M.S. Thesis, Graduate School of Civil, Mechanical, and Environmental Engineering, George Washington Univ., Washington, DC, Sept. 1990.